

Cavity-assisted single-shot T center spin readout

Yu-En Wong

*Department of Electrical and Computer Engineering, Rice University, Houston, TX 77005, USA and
Applied Physics Graduate Program, Smalley-Curl Institute, Rice University, Houston, TX 77005, USA*

Songtao Chen*

*Department of Electrical and Computer Engineering, Rice University, Houston, TX 77005, USA and
Smalley-Curl Institute, Rice University, Houston, TX 77005, USA*

(Dated: October 31, 2025)

High-fidelity spin readout is a crucial component for quantum information processing with optically interfaced solid-state spins. Here, we propose and investigate two theoretical protocols for fast single-shot readout of cavity-coupled single T center electronic spins. For fluorescence-based readout, we selectively couple one of the T center spin-conserving transitions to a single-mode photonic cavity, exploiting the enhancement of the fluorescence emission and cyclicity. For reflection-based readout, we leverage the spin-dependent cavity reflection contrast to generate the qubit readout signal. We show that the cavity reflection approach enables high-fidelity spin readout even when the T center only has a modest cyclicity. With realistic system parameters, such as cavity quality factor $Q = 2 \times 10^5$ and T center optical linewidth $\Gamma/2\pi = 100$ MHz, we calculate a single-shot readout fidelity exceeding 99% within 8.7 μ s for both spin readout protocols.

I. INTRODUCTION

Optically interfaced solid-state spins have been widely used for a variety of quantum technologies [1], including quantum interconnect and networking. These spin systems can store quantum information locally in individually addressable particles and send out spin-entangled photons for networking applications. Using mature solid-state spin platforms such as quantum dots and defect centers in diamond (e.g., NV, SiV), efficient spin-photon entanglement [2–4] and remote spin entanglement [5, 6] have been demonstrated. Quantum frequency conversion is commonly used in these platforms to convert the wavelength to telecom-band for long-range applications [7, 8]. Single erbium ions in oxide materials provide spin-photon interfaces at telecom-C band [9], with spin-photon entanglement demonstrated recently [10].

Radiation damage centers are another family of defects that offer telecom-band optical emission and scalable photonic and electronic device integration in the mature silicon material platform [11, 12]. Single T centers are particularly promising optically active spins in silicon (OASIS) for building quantum network nodes and repeater devices due to their telecom-O band optical transition ($\lambda = 1326$ nm) and the long-lived doublet spin manifold in the ground state [13]. Several recent works have demonstrated single T center isolation and silicon photonic device integration [14–18], as well as coherent coupling to the nearby nuclear spins [19].

An important requirement for quantum information processing using solid-state spins is the high-fidelity single-shot spin readout. Based on the cavity-enhanced fluorescence enabled by the cavity quantum electrodynamics (cQED), single-shot spin measurements have

been achieved in a variety of solid-state spin platforms, including quantum dots [20, 21], NV [22] and SiV [23] centers in diamond, as well as rare earth ions [24, 25]. High-fidelity spin readout based on resonant fluorescence relies on the highly cyclic optical transitions to scatter sufficient photons for detection before spin flips. Cycling transition can be enabled by intrinsic atomic selection rules [21], tuning transition dipole alignment with an external magnetic field [23, 26], or by tailoring the electromagnetic density of states via a cavity [24, 25]. Leveraging cQED in the intermediate- and high-cooperativity regime, spin-modulated cavity reflection or transmission has been used to perform high-fidelity single-shot spin readout in SiV [4, 27, 28]. Moreover, spin-to-charge conversion is also utilized to enable single-shot spin readout [29, 30]. For T centers in silicon, high-fidelity single-shot readout has been demonstrated for the ${}^1\text{H}$ nuclear spin [31], however, the same readout task for single T center electronic spins remains elusive.

In this work, we propose two cQED protocols to perform single-shot readout of the T center electronic spin. We first construct our theoretical framework based on a four-level system with two ground spin states ($S = 1/2$) forming the qubit, and two Zeeman-split optically excited states, coupled to a low-loss, small mode volume, and single-mode optical cavity. We then analyze the spin readout performance using two cQED protocols based on resonant fluorescence and cavity reflection. Under realistic experimental conditions and system parameters, we calculate the spin readout fidelity by thresholding the probability distribution of spin-dependent photon detections. We show that a 99.96% fidelity can be realized in fluorescence-based readout, although it requires high cyclicity, short laser excitation pulses, and high-efficiency detection of fast resonant fluorescence. By using spin-modulated cavity reflection, even with a modest cyclicity, we show that a 99.6% readout fidelity can be achieved.

* songtao.chen@rice.edu

The paper is organized as follows: Sec. II describes the theoretical framework for the protocols; Sec. III and Sec. IV analyze the performance of the fluorescence-based and reflection-based spin readout, respectively. In Sec V, we will further investigate the impact of spectral diffusion on the readout fidelity.

II. OPEN QUANTUM SYSTEM: LINDBLADIAN FORMALISM

We consider a cavity-coupled single T center under a static magnetic field, which lifts the spin degeneracy in both the ground and excited states (Fig. 1), revealing four distinct optical transitions. Transition A and B conserve the spin, while C and D flip the spin. The system Hamiltonian is based on the extended Jaynes-Cummings model, which considers 4 levels interacting with the single-mode cavity field. The single sided cavity output field (Fig. 1a) is described by the input-output relation (Sec. IV).

We write the system Hamiltonian in a reference frame with respect to the frequency of incident field ω_L , given by $\mathbf{H}/\hbar = \mathbf{H}_0 + \mathbf{H}_{\text{int}} + \mathbf{H}_d$:

$$\mathbf{H}_0 = \Delta_c \mathbf{a}^\dagger \mathbf{a} + \Delta_g (\boldsymbol{\sigma}_{11} - \boldsymbol{\sigma}_{00}) + (\Delta_a - \Delta_e) \boldsymbol{\sigma}_{22} + (\Delta_a + \Delta_e) \boldsymbol{\sigma}_{33} \quad (1)$$

$$\mathbf{H}_{\text{int}} = g_{\parallel} (\boldsymbol{\sigma}_{31} + \boldsymbol{\sigma}_{20}) \mathbf{a}^\dagger + g_{\perp} e^{i\phi} (\boldsymbol{\sigma}_{30} + \boldsymbol{\sigma}_{21}) \mathbf{a}^\dagger + h.c. \quad (2)$$

$$\mathbf{H}_d = \sqrt{\kappa \eta_{\text{cav}} \epsilon} (\mathbf{a}^\dagger + \mathbf{a}) \quad (3)$$

where $|0\rangle, |1\rangle, |2\rangle, |3\rangle$ represent $|\downarrow_g\rangle, |\uparrow_g\rangle, |\downarrow_e\rangle, |\uparrow_e\rangle$ levels (Fig. 1b), respectively; $\boldsymbol{\sigma}_{ij} = |j\rangle \langle i|$ with $i, j = 0, 1, 2, 3$; $\mathbf{a}^\dagger(\mathbf{a})$ is the photonic creation (annihilation) operators; $\Delta_a = \omega_a - \omega_L$ and $\Delta_c = \omega_c - \omega_L$ are the detunings between the bare atomic (ω_a), cavity (ω_c) and laser (ω_L) frequencies; $2\Delta_g$ and $2\Delta_e$ are the ground and excited state Zeeman splitting; g_{\parallel} and g_{\perp} are the atom-cavity coupling strengths for spin-conserving and spin-non-conserving transitions, with their ratio defined as $r_g = g_{\parallel}/g_{\perp}$. The phase difference ϕ between two couplings originated from the alignment between the external magnetic field and the T center spin quantization axis. Our calculations suggest a negligible influence of this phase on the readout fidelity and we keep $\phi = \pi/2$ in the fidelity analysis. $2g = 2\sqrt{g_{\parallel}^2 + g_{\perp}^2}$ is the single-photon Rabi frequency for the bare T center; $\epsilon = P_{\text{in}}/(\hbar\omega_L)$ is the input excitation photon flux, where P_{in} is the input laser power right before entering the cavity; κ is the total cavity loss rate and $\eta_{\text{cav}} = \kappa_{\text{wg}}/\kappa$ is the efficiency for cavity decay into the waveguide (κ_{wg}). Due to the small hyperfine interaction compared to the intrinsic and the cavity-enhanced optical linewidths, we ignore ${}^1\text{H}$ nuclear spin levels in the model.

The time evolution of the system dynamics is described

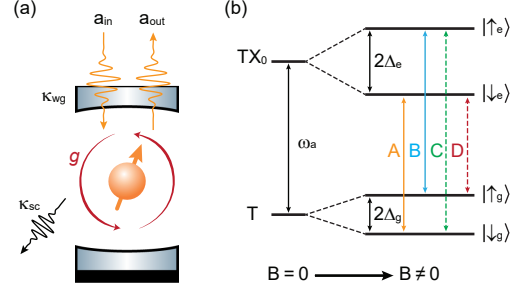


FIG. 1. **Proposed cQED scheme for the T center electronic spin readout.** (a) Illustration of a single T center coupled to a one-sided cavity, where the input and output laser fields ($\mathbf{a}_{\text{in}}, \mathbf{a}_{\text{out}}$) couple to the cavity mode at a rate of κ_{wg} . The cavity scattering loss rate κ_{sc} is also included. The coupling rate between the single T center and the cavity mode is given by g at zero field. (b) A simplified energy diagram is shown on the right. Four transitions emerge after an external magnetic field B is applied. The Zeeman splittings for ground and excited states are $2\Delta_e$ and $2\Delta_g$, respectively.

by Lindblad master equation:

$$\dot{\rho} = \frac{-i}{\hbar} [\mathbf{H}, \rho] + \sum_i \mathbf{c}_i \rho \mathbf{c}_i^\dagger - \frac{1}{2} \{ \mathbf{c}_i^\dagger \mathbf{c}_i, \rho \} \quad (4)$$

where \mathbf{c}_i are the collapse operators describing the interaction with the environment (Table. I).

TABLE I. Collapse operators considered in the Lindbladian. We use balanced transition rates for $\boldsymbol{\sigma}_{20(31)}$ and $\boldsymbol{\sigma}_{21(30)}$ [14] in the calculation. Γ_d is the pure dephasing rate.

Loss channel	Operator
Cavity decay	$\sqrt{\kappa} \mathbf{a}$
Excited state dephasing	$\sqrt{\Gamma_d/2} \boldsymbol{\sigma}_{z1}; \sqrt{\Gamma_d/2} \boldsymbol{\sigma}_{z2}$ ^a
Spin-conserving SPE ^b	$\sqrt{\Gamma_0/2} \boldsymbol{\sigma}_{31}; \sqrt{\Gamma_0/2} \boldsymbol{\sigma}_{20}$
Spin-nonconserving SPE	$\sqrt{\Gamma_0/2} \boldsymbol{\sigma}_{30}; \sqrt{\Gamma_0/2} \boldsymbol{\sigma}_{21}$

^a $\boldsymbol{\sigma}_{z1} = \boldsymbol{\sigma}_{22} - \boldsymbol{\sigma}_{00}; \boldsymbol{\sigma}_{z2} = \boldsymbol{\sigma}_{33} - \boldsymbol{\sigma}_{11}$

^b Spontaneous emission

To investigate the dynamics of the open quantum system, we solve the master equation numerically with the system Hamiltonian shown above with QuTip [32]. The obtained atomic and cavity excitations are used to calculate the detected photons and infer the spin readout fidelity. The optical linewidth $\Gamma = \Gamma_0 + 2\Gamma_d$ consists of a Fourier-limited linewidth $\Gamma_0 = 2\pi \times 169.3$ kHz [13] and pure dephasing Γ_d . Extra linewidth broadening can result from spectral diffusion and affect spin readout performance (Sec. V). Based on this theoretical framework, we investigate two cQED spin readout protocols via resonant fluorescence (Sec. III) and spin-dependent cavity reflection (Sec. IV).

III. SPIN READOUT VIA RESONANT FLUORESCENCE

The branching ratio for bulk T centers is relatively balanced [14], leading to a low cyclicity and fast electronic spin polarization under optical excitations. We integrate single T centers with a low-loss, small mode volume optical cavity, which can selectively enhance the spin-conserving optical decay pathways [24], enabling cyclic transitions to collect sufficient fluorescence photons before spin flips.

To perform the T center spin readout via resonant fluorescence, we align the cavity and the resonant laser excitation with one of the spin-conserving transitions, e.g., transition A (Fig. 2a, inset). A short laser excitation (pulse width of t_{pulse}) resonantly excites the T center and the fluorescence is subsequently collected for a duration of $t_{\text{wait}} = 7\tau_{\text{cav}}^{\text{off}}$, where $\tau_{\text{cav}}^{\text{off}}$ is the fluorescence lifetime for the other spin-conserving transition that is off-resonant with the cavity. This practice is chosen to ensure the excited state population fully decays after each excitation pulse regardless of the initialized spin state, which enables us to extract the cyclicity accurately. We repeat the excite-collect sequence (length of $t_{\text{seq}} = t_{\text{pulse}} + t_{\text{wait}}$) N_{cyc} (defined below) times to collect fluorescence photons for spin readout. Depending on the T center spin state, different intensity of fluorescence will be obtained (Fig. 2a). We gate our single photon detector in the time-domain to avoid detector latching due to the strong laser excitation pulse [15].

The number of collected fluorescence photons (N_{ph}) can be calculated as,

$$N_{\text{ph}} = \beta_{\text{cav}} \eta_{\text{sys}} \sum_{n=0}^{N_{\text{cyc}}-1} P_e(P_g)^n, \quad (5)$$

where P_e is the excited state population at the end of the laser excitation pulse ($t = t_{\text{pulse}}$) and P_g is the ground state population at the end of the first excite-collect sequence ($t = t_{\text{seq}}$), assuming a perfect initialization process. Note that P_g and P_e correspond to states within a spin-conserving transition defined by the initialized spin state. $\beta_{\text{cav}} = (\Gamma_{\text{cav}} - \Gamma_0)/\Gamma_{\text{cav}}$ is the portion of T center emission coupled to the cavity mode, with Γ_{cav} and Γ_0 being the T center fluorescence decay rate with and without cavity coupling, respectively. $\eta_{\text{sys}} = \eta_{\text{cav}} \eta_{\text{det}} = 13.8\%$ is the total system efficiency [15], where $\eta_{\text{det}} = 27.5\%$ contains efficiencies for grating coupler, fiber network, and single photon detection. Note that we target at $\eta_{\text{cav}} = 50\%$ for maximal outcoupling of T center fluorescence [33]. Other relevant system parameters are listed in Table II. Due to the finite cyclicity, the initialized ground state population will eventually be optically pumped away, leading to the decrease of fluorescence counts per excitation pulse (Fig. 2b, inset). The decay is described by the term $(P_g)^n \approx \exp(-(1-P_g)n)$, considering $P_g \approx 1$. We thus choose the sequence repetition $N_{\text{cyc}} = (1 - P_g)^{-1}$, which is the corresponding

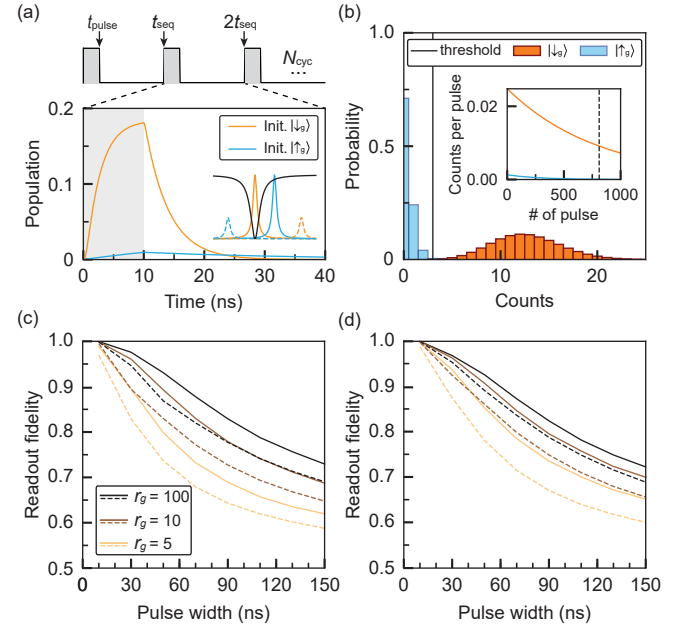


FIG. 2. Spin-dependent fluorescence readout. (a) Excited state population dynamics with different initialized states. The gray shaded region represents the square laser pulse with the readout sequence shown in the top panel. The inset shows the cavity (black line) alignment with the transition A. (b) Poissonian distribution $P(N_{\text{ph}}, k)$ of detected fluorescence photon counts under different spin initializations. The inset shows the average photon counts per pulse decay due to the optical pumping. The number of excitation pulses N_{cyc} for readout is chosen to be $1/e$ decay point (black dashed line). Simulation parameters for panel a and b: $Q = 1 \times 10^5$, $\Gamma/2\pi = 1$ GHz, $t_{\text{pulse}} = 10$ ns, $P_{\text{in}} = 100$ pW, and $r_g = 10$. Both the cavity and the laser are tuned resonant with the transition A. (c) and (d) r_g dependence of readout fidelity with cavity $Q = 1 \times 10^5$ (c) and $Q = 2 \times 10^5$ (d). In both panels, solid and dashed lines represent $\Gamma/2\pi = 0.1$ GHz and $\Gamma/2\pi = 1$ GHz, respectively. Other system parameters can be found in Table II.

optical transition cyclicity. Considering the large splitting between the two spin-conserving transitions (4 GHz) against the cavity linewidth used in the calculation and

TABLE II. Global parameters considered in the readout fidelity calculation. We use the lower bound of T center quantum efficiency [15]. g_e and g_h are the ground and excited state g-factors, respectively; μ_B is the Bohr magneton and B is the external magnetic field. The atom-cavity coupling $g = g_{\text{sim}} \sqrt{\eta Q E}$ assuming ideal T center positioning and dipole alignment with the cavity field.

Symbol	Value	Description
$ g_e - g_h \mu_B B$	4 GHz	splitting between transition A and B
$g_{\text{sim}}/2\pi$	376 MHz	simulated coupling strength
η_{QE}	0.234	quantum efficiency

the long spin T_1 lifetime for T centers [13], we ignore the minor fluorescence contribution resulted from the opti-

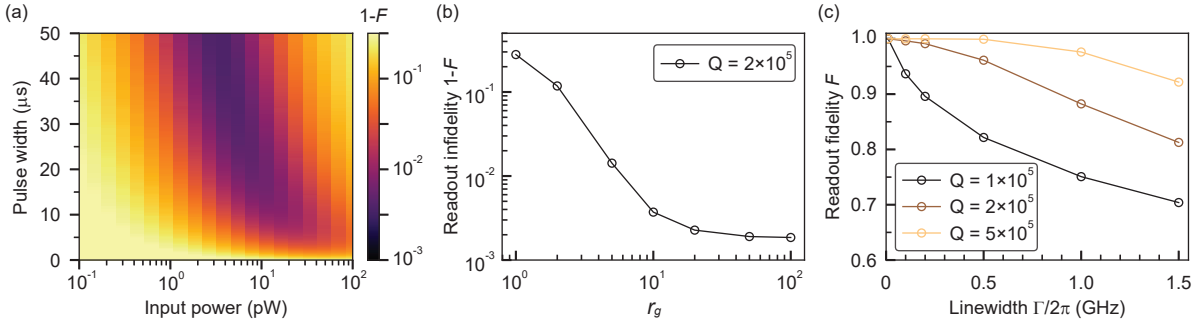


FIG. 3. Spin-dependent cavity reflection readout. (a) Spin readout infidelity calculations under different laser input powers and pulse widths with optimized Δ_a and Δ_c maximizing the reflection contrast. Lower laser powers necessitate longer pulses for reaching the maximal fidelity. System parameters used are listed in Table. III. (b) Extracted minimum readout infidelity in panel (a) with different r_g while keeping other system parameters the same. Saturation behavior happens for $r_g \geq 5$. (c) The maximum readout fidelity under different system parameters (Q , Γ) with $t_{\text{pulse}} \leq 50 \mu\text{s}$ and $0.1 \leq P_{\text{in}} \leq 100 \text{ pW}$.

cally pumped away population. We choose a relatively low optical excitation power $P_{\text{in}} = 100 \text{ pW}$, corresponding to $\sim 0.1P_{\text{sat}}$ with P_{sat} being the saturation pump power, to minimize laser-induced excited state spin mixing [34] and spectral diffusion [34, 35].

Given the cavity and laser frequency location, the measurement of spin-dependent fluorescence yields two Poissonian distributions ($P(N_{\text{ph}}, k)$) with different mean photon number (N_{ph}) depending on the initialized spin state (Fig. 2b). The spin readout fidelity is given by,

$$F = \frac{1}{2} \left[P(N_{\text{ph}}^{|\uparrow_g\rangle}, k < M) + 0.5P(N_{\text{ph}}^{|\uparrow_g\rangle}; k = M) \right. \\ \left. + P(N_{\text{ph}}^{|\downarrow_g\rangle}, k > M) + 0.5P(N_{\text{ph}}^{|\downarrow_g\rangle}, k = M) \right], \quad (6)$$

where $N_{\text{ph}}^{|\uparrow_g\rangle}$ and $N_{\text{ph}}^{|\downarrow_g\rangle}$ are the mean detected photon numbers when the spin state is initialized to $|\uparrow_g\rangle$ and $|\downarrow_g\rangle$, respectively; M is the photon number threshold that maximize the readout fidelity. Figure. 2c, d summarize spin readout fidelity via resonant fluorescence, depending on system parameters of r_g , Γ , Q , and t_{pulse} . High r_g facilitates more cyclic optical transitions, leading to better fluorescence contrast and thus higher spin readout fidelity. The cyclicity is further boosted by narrower optical cavity (i.e. higher Q) and T center optical transition linewidths, which enable larger Purcell enhancement contrast between the resonant transition A and other detuned transitions. Longer optical excitation pulse width significantly deteriorates the fidelity, which results from the spin-flipping fluorescence decay ($\Gamma_0/2$) during the optical excitation process and lowers the effective cyclicity. Short optical excitation ($t_{\text{pulse}} \lesssim 30 \text{ ns}$) is required to minimize such an effect. With realistic near-term system parameters shown in Table. III and laser excitation pulses with $t_{\text{pulse}} = 10 \text{ ns}$ and $P_{\text{in}} = 100 \text{ pW}$, spin readout fidelity $F = 99.96\%$ can be achieved with a readout time of $179 \mu\text{s}$. By choosing $t_{\text{wait}} = 7\tau_{\text{cav}}^{\text{on}}$, where $\tau_{\text{cav}}^{\text{on}}$ is the cavity-enhanced fluorescence lifetime for the transition that is resonant with the cavity, a much faster readout time of $8.7 \mu\text{s}$ can be realized with $F = 99.97\%$. We note

that collecting resonant fluorescence with a short decay lifetime can be technically challenging due to the filtering of the laser excitation.

IV. SPIN READOUT VIA CAVITY REFLECTION

Next, we turn to the protocol based on spin-dependent cavity reflection for spin readout. The single-sided cavity output field is described by the input-output relation [36],

$$\mathbf{a}_{\text{out}} = \mathbf{a}_{\text{in}} + \sqrt{\kappa_{\text{wg}}} \mathbf{a}, \quad (7)$$

where \mathbf{a}_{in} and \mathbf{a}_{out} are the cavity-coupled input and output laser fields, respectively. The input laser field is given by $\mathbf{a}_{\text{in}} = i\sqrt{\epsilon}$. We compute the cavity reflectivity numerically by solving the master equation for given detunings and T center spin states using

$$R = \left| \frac{\langle \mathbf{a}_{\text{out}} \rangle}{\langle \mathbf{a}_{\text{in}} \rangle} \right|^2, \quad (8)$$

A global optimization [37] is implemented to locate cavity (Δ_c) and atomic (Δ_a) detunings under a weak excitation condition [38] to maximize the contrast of the spin-dependent cavity reflection (See Appendix. A). The cavity-reflected photon number (N_{ph}) upon a laser pulse (t_{pulse}) radiation can be calculated by integrating the photon output flux of the cavity over the time duration of the laser pulse,

$$N_{\text{ph}} = \eta_{\text{det}} \int_0^{t_{\text{pulse}}} |\langle \mathbf{a}_{\text{in}} \rangle + \sqrt{\kappa_{\text{wg}}} \text{Tr}[\rho(t)\mathbf{a}]|^2 dt, \quad (9)$$

where $\rho(t)$ is the density matrix of the system (Eq. 4). Different T center spin states lead to a contrast of average reflected photon numbers, the distributions of which are utilized to infer the spin readout fidelity using Eq. 6.

We first investigate the spin readout performance with the realistic experimental parameters listed in the Table. III, which leads to an atomic cooperativity $C =$

$4g^2/(\kappa\Gamma) = 1.2$. The maximal readout fidelity for the cavity reflection protocol has a weak dependence on the cavity efficiency η_{cav} (Appendix A) and we keep $\eta_{\text{cav}} = 50\%$ the same with that used in the fluorescence readout. Figure 3a demonstrates the readout fidelity with a bounded laser pulse width of $t_{\text{pulse}} \leq 50 \mu\text{s}$ and laser power $0.1 \leq P_{\text{in}} \leq 100 \text{ pW}$. The maximal readout fidelity $F = 99.6\%$ can be achieved with $t_{\text{pulse}} = 47 \mu\text{s}$ and $P_{\text{in}} = 3.8 \text{ pW}$. On the other hand, faster spin readout is possible with higher laser powers, which can reach $F = 99.0\%$ with $P_{\text{in}} = 16 \text{ pW}$ and $t_{\text{pulse}} = 8.7 \mu\text{s}$ (same as the fluorescence readout). We note that longer pulses and higher powers will cause optical pumping and spin flipping, which can deteriorate the spin readout fidelity performance. Lower laser powers necessitate longer pulse width to reach the maximal fidelity (Appendix B). Tradeoff between fidelity and readout duration is needed for different applications.

The cavity reflection-based readout has a less demanding requirement on the ratio r_g (Fig. 3b) compared to the resonance fluorescence-based readout due to the lower power operation and less involvement of the optical excited states. The reflection readout depends strongly on the cooperativity, where higher readout fidelity can be achieved with larger cavity quality factors and narrower T center optical linewidths (Fig. 3c). With $C > \sim 0.3$, a readout fidelity $> 90\%$ can be obtained. Compared to the fluorescence-based readout, the reflection-based readout holds a few technical advantages by mitigating the requirements of generating short laser pulses and fast time-domain filtering of the laser excitations.

TABLE III. Near-term targeted system parameters.

Symbol	Value	Description
Q	2×10^5	cavity Q factor
$\Gamma/2\pi$	0.1 GHz	optical linewidth
r_g	10	coupling strength ratio

V. OPTICAL DEPHASING AND SPECTRAL DIFFUSION

In this section, we investigate the influence of the spectral diffusion on the two spin readout protocols. Even though T center emission stays stable in the dark up to $\sim \text{ms}$, they have been shown to suffer from laser-induced spectral diffusion [34, 35]. Based on photon correlation measurements, single T center spectral diffusion time scale has been measured on the order of tens of μs [15, 34]. We have included T center optical transition broadening due to the pure dephasing for both excited states $|\downarrow_e\rangle$ and $|\uparrow_e\rangle$ via the jump operators $\sqrt{\Gamma_d/2}\sigma_{z1}$ and $\sqrt{\Gamma_d/2}\sigma_{z2}$, respectively, in the master equation beyond the lifetime limited linewidth (Γ_0), revealing dephasing broaden linewidth $\Gamma = \Gamma_0 + 2\Gamma_d$. Considering the spectral diffusion time scale is comparable or longer than the repetition time of a readout measurement, we

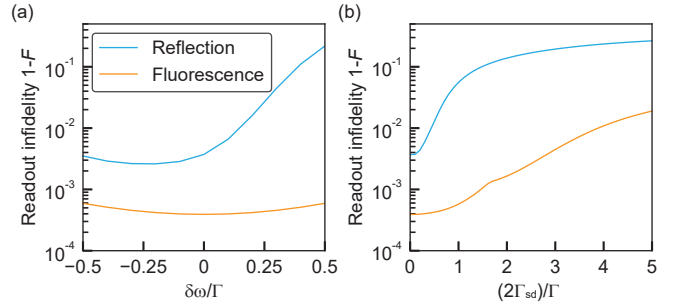


FIG. 4. Effect of spectral diffusion on spin readout. (a) Readout infidelity at different optical transition detunings ($\delta\omega$) in two protocols. For each spectral detuning $\delta\omega$, all other system and readout parameters are kept the same as the case when $\delta\omega = 0$ in the calculation. The reflection-based readout shows an asymmetric infidelity profile, which results from the larger reflection contrast decrease and optical pumping with positive detunings. (b) Readout infidelity for the two protocols under the spectral diffusion manifested as a random spectral wandering, which is modeled as a Gaussian distribution with a FWHM of $2\Gamma_{\text{sd}}$. Gaussian-weighted average of the detected photon distributions at different $\delta\omega$ are used to calculate the spin readout fidelity. For both panel (a) and (b), the results are derived with cQED parameters listed in Table. III. Fluorescence-based readout utilizes $t_{\text{pulse}} = 10 \text{ ns}$ and $P_{\text{in}} = 100 \text{ pW}$ while the reflection-based readout uses $t_{\text{pulse}} = 47 \mu\text{s}$ and $P_{\text{in}} = 3.8 \text{ pW}$. Both $\delta\omega$ and $2\Gamma_{\text{sd}}$ are presented in units of the fast dephasing broadend linewidth $\Gamma/2\pi = 0.1 \text{ GHz}$.

simplify the diffusion process during spin readout by assuming $\omega_a = \omega_a^0 + \delta\omega$, with ω_a^0 being the average of the bare atomic transition and $\delta\omega$ being a random variable which may be different for each measurement shot. The distribution of the detected photon counts can be evaluated as,

$$\text{Dist}(k) = \int P(\mu(\delta\omega), k)G(\delta\omega)d\delta\omega, \quad (10)$$

where $P(\mu(\delta\omega), k)$ is the Poissonian distribution with a mean photon count $\mu(\delta\omega)$, depending on the spectral diffusion value $\delta\omega$ at a specific measurement shot. The spectral diffusion is modeled as a Gaussian distribution,

$$G(\delta\omega) = \frac{1}{\Gamma_{\text{sd}}} \sqrt{\frac{\ln 2}{\pi}} \exp \left[-\ln 2 \left(\frac{\delta\omega}{\Gamma_{\text{sd}}} \right)^2 \right], \quad (11)$$

where $2\Gamma_{\text{sd}}$ is the full-width-half-maximum (FWHM) of the broadening due to the spectral diffusion.

The spectral diffusion of the T center optical transition causes the readout infidelity to increase in both protocols (Fig. 4a). In the fluorescence-based readout, detuning between the cavity and the spin-conserving transition lowers Purcell enhancement and subsequent fluorescence counts. In the reflection-based readout, deviation of $\Delta_{ac} = \Delta_a - \Delta_c$ from its optimal value decreases the reflection contrast, causing the increase of readout infidelity. We note the asymmetric infidelity profile in the

reflection-based readout, which comes from the interplay between optical pumping effect and contrast changing at different $\delta\omega$ (Appendix A). Under the spectral diffusion, the detected photon count distributions for different initialized spin states are obtained by the Gaussian weighted averages of the readout trials with different $\delta\omega$ (Eq. 10 and Eq. 11). Same thresholding method (Eq. 6) is applied to infer the readout fidelity (Fig. 4b). The fluorescence-based readout is more resilient to the spectral diffusion thanks to the large Purcell enhancement contrast between the near-resonant and off-resonant optical transitions. The reflection-based readout suffers more from the spectral diffusion due to the fast decrease of the cavity reflection contrast beyond the T center cavity-enhanced optical linewidth (Appendix A).

VI. DISCUSSION AND CONCLUSION

Now we discuss limiting factors and pathways to reach the theoretical readout performance in experiments. The fluorescence-based readout requires high transition cyclicity, which can be enhanced by optimizing alignment between the external magnetic field and the cavity polarization [24]. To collect the fast resonant fluorescence signal ($< \sim 10$ ns) and filter out the laser excitations, spatial filtering can be utilized to improve the existing time-domain filtering method via gating the detector. Both protocols necessitate a narrow T center optical linewidth (Γ) and a large atom-cavity coupling strengths (g), as well as a low-loss optical cavity (κ). For the optical linewidth, electrical field control may be used to minimize spectral diffusion of cavity-coupled T centers via depletion of the charge noises. The same technique was demonstrated for divacancies in SiC, achieving linewidth narrowing by a factor of 30 [39]. The lower power operation (\sim pW) in the cavity reflection-based readout can benefit the optical linewidth by minimizing the environmental charge reconfiguration due to the excitation laser [34, 35]. To promote higher coupling constant g , we note that focused-ion-beam-based [40] and masked [41] ion implantation can be leveraged to increase the yield of T center generation at the cavity center.

In summary, we have proposed and investigated two protocols for single-shot spin readout of cavity-coupled T center electronic spins via resonant fluorescence and spin-modulated cavity reflection. Both protocols can enable fast readout (~ 10 μ s) and reach fidelity $F > 99\%$ with realistic system parameters, which put them among the state-of-the-art spin readout performance achieved in the solid-state defects [28, 42, 43]. The high fidelity single-shot spin readout is an enabling step towards a broad range of T-center-spin-based quantum information applications [31]. The proposed computation framework can be utilized for exploring other cQED-enabled quantum optical control for T centers such as cavity-mediated spin-spin interactions [27] and cavity-enhanced Raman emission [44].

DATA AVAILABILITY

The datasets generated and/or analyzed during the current study are available from the corresponding author on reasonable request.

ACKNOWLEDGMENTS

We gratefully acknowledge Qiyang Huang, Adam Johnston, Shuo Sun, Yizhi Zhu and Geoffroy Hautier for helpful discussions. Support for this research was provided by the National Science Foundation CAREER Award (No. 2238298) and Electronics, Photonics and Magnetic Devices (EPMD) program (No. 2527905), as well as the Robert A. Welch Foundation (Grant No. C-2134).

Appendix A: REFLECTION CONTRAST AT DIFFERENT CAVITY EFFICIENCY

Cavity efficiency $\eta_{\text{cav}} = \kappa_{\text{wg}}/\kappa$ quantifies cavity decay rate through the waveguide mode over the total cavity decay, which can be tuned during nanofabrication. η_{cav} determines how efficiently the input laser field is coupled to the cavity mode and subsequently interacts with the T center. In this section, we look into the influence of the η_{cav} on the performance of the reflection-based spin readout with system parameters listed in Table III. First, we analyze the maximal reflection contrast (Fig. 5a) via a global optimization process [37] of Δ_a and Δ_c , which reveals a monotonic increase for $\eta_{\text{cav}} \geq 0.5$. However, we note a deviation from the above trend for $\eta_{\text{cav}} < 0.5$. To explain such a discontinuous trend, we turn to an analytical model for cavity reflection under the weak excitation condition [38],

$$r = \frac{\langle \mathbf{a}_{\text{out}} \rangle}{\langle \mathbf{a}_{\text{in}} \rangle} \approx 1 - \frac{\kappa \eta_{\text{cav}}}{\kappa/2 + i\Delta_c + \frac{g^2}{i\Delta_a + \Gamma/2}}. \quad (\text{A1})$$

Figure. 5b shows the spin-dependent cavity reflection with optimized Δ_a and Δ_c with different η_{cav} . For $\eta_{\text{cav}} < 0.5$, the maximal reflection contrast is achieved when the cavity is aligned with one of the spin-conserving transitions (e.g., transition A), benefiting from the vacuum Rabi splitting. While for $\eta_{\text{cav}} \geq 0.5$, the maximal contrast is achieved in the dispersive regime when the cavity is detuned from the transition A. The change of the regime causes the discontinuity in the contrast profile at $\eta_{\text{cav}} = 0.5$. If forcing the cavity always align with the transition A, the discontinuity of the contrast profile vanishes (Fig. 5a).

Next, we calculate the maximal readout fidelity at different η_{cav} , which all reach $> 99.6\%$ for the given range of laser power and pulse width used in Section IV, and the results have a weak dependence on η_{cav} . The higher η_{cav}

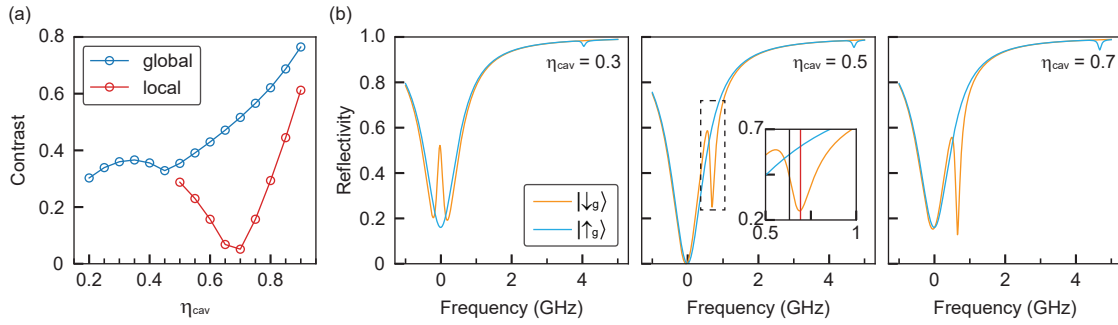


FIG. 5. Contrast with different cavity efficiency η_{cav} . (a) The blue curve is derived from global optimization process of Δ_a and Δ_c ; the red curve is obtained by aligning the cavity with one of the spin-conserving transitions. (b) Optimized spin-dependent cavity reflection curves with different η_{cav} . All blue (orange) curves represent initialized spin state to be $|\uparrow_g\rangle$ ($|\downarrow_g\rangle$). For $\eta_{\text{cav}} = 0.5$ (middle panel), the black line in the inset marks the location of the optical transition A, while the red line shows the maximal contrast point. The separation between the two is due to the dispersive shift.

facilitates lower laser power operation due to the more efficient cavity-waveguide coupling. In quantum information applications, critically-coupled cavity ($\eta_{\text{cav}} = 0.5$) can improve the spin-photon entanglement fidelity [4, 28] while over-coupled cavity ($\eta_{\text{cav}} > 0.5$) can enable efficient spin-dependent phase flip for spin readout [45].

Appendix B: LONGER LASER PULSE IN REFLECTION-BASED READOUT

In the reflection-based readout (Section IV), given the system parameters, the input laser power and pulse width determine the readout fidelity (Fig. 3a), where the pulse width is chosen to be bounded below 50 μs to enable fast single-shot readout. Here, we investigate how longer laser pulse width can affect the readout performance. For a specific laser power, longer laser pulse helps accumulate reflected photons, which promotes the readout fidelity given the reflection contrast. However, due to the optical pumping, the longer probing laser pulse will eventually induce a spin flip, decreasing the readout fidelity (Fig. 6). For example, at a high laser power ($P_{\text{in}} = 23.4$ pW), the readout reaches a fidelity of 98.9% with a pulse width of 11 μs . Further increase of the pulse width decreases the fidelity. Such an optimal pulse width point moves to longer values and the maximal readout fidelity

saturates at 99.7% under lower laser powers (Fig. 6) given the 200 μs pulse width bound. For spin readout measurements in experiments, trade off needs to be made between readout fidelity and speed for different applications.

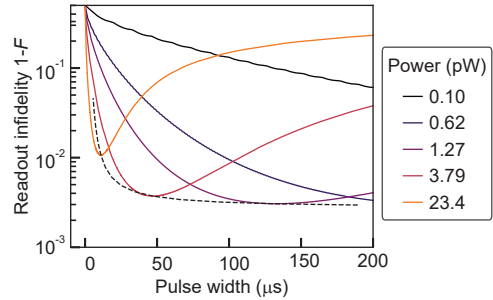


FIG. 6. Reflection-based readout with longer laser pulses. Calculated readout infidelity for reflection-based readout with different laser powers and pulse widths, with other system parameters specified in Table III. Lower laser power requires a longer laser pulse to accumulate sufficient photon counts for reaching the optimal fidelity. The black dashed line shows the minimal infidelity at each power for $t_{\text{pulse}} \leq 200 \mu\text{s}$.

-
- [1] D. D. Awschalom, R. Hanson, J. Wrachtrup, and B. B. Zhou, Quantum technologies with optically interfaced solid-state spins, *Nat. Photon.* **12**, 516 (2018).
- [2] E. Togan, Y. Chu, A. S. Trifonov, L. Jiang, J. Maze, L. Childress, M. G. Dutt, A. S. Sørensen, P. R. Hemmer, A. S. Zibrov, *et al.*, Quantum entanglement between an optical photon and a solid-state spin qubit, *Nature* **466**, 730 (2010).
- [3] W. Gao, P. Fallahi, E. Togan, J. Miguel-Sánchez, and A. Imamoglu, Observation of entanglement between a quantum dot spin and a single photon, *Nature* **491**, 426 (2012).
- [4] C. Nguyen, D. Sukachev, M. Bhaskar, B. Machielse, D. Levonian, E. Knall, P. Stroganov, C. Chia, M. Burek, R. Riedinger, *et al.*, An integrated nanophotonic quantum register based on silicon-vacancy spins in diamond, *Phys. Rev. B* **100**, 165428 (2019).
- [5] H. Bernien, B. Hensen, W. Pfaff, G. Koolstra, M. S. Blok, L. Robledo, T. H. Taminiau, M. Markham, D. J. Twitchen, L. Childress, *et al.*, Heralded entanglement be-

- tween solid-state qubits separated by three metres, *Nature* **497**, 86 (2013).
- [6] W. Pfaff, B. J. Hensen, H. Bernien, S. B. van Dam, M. S. Blok, T. H. Taminiau, M. J. Tiggelman, R. N. Schouten, M. Markham, D. J. Twitchen, *et al.*, Unconditional quantum teleportation between distant solid-state quantum bits, *Science* **345**, 532 (2014).
- [7] K. De Greve, L. Yu, P. L. McMahon, J. S. Pelc, C. M. Natarajan, N. Y. Kim, E. Abe, S. Maier, C. Schneider, M. Kamp, *et al.*, Quantum-dot spin–photon entanglement via frequency downconversion to telecom wavelength, *Nature* **491**, 421 (2012).
- [8] C. M. Knaut, A. Suleymanzade, Y.-C. Wei, D. R. Assumpcao, P.-J. Stas, Y. Q. Huan, B. Machielse, E. N. Knall, M. Sutula, G. Baranes, *et al.*, Entanglement of nanophotonic quantum memory nodes in a telecom network, *Nature* **629**, 573 (2024).
- [9] A. Dibos, M. Raha, C. Phenicie, and J. D. Thompson, Atomic source of single photons in the telecom band, *Phys. Rev. Lett.* **120**, 243601 (2018).
- [10] M. T. Uysal, L. Dusanowski, H. Xu, S. P. Horvath, S. Ourari, R. J. Cava, N. P. De Leon, and J. D. Thompson, Spin-photon entanglement of a single er^{3+} ion in the telecom band, *Phys. Rev. X* **15**, 011071 (2025).
- [11] C. E. Jones, E. S. Johnson, W. D. Compton, J. Noonan, and B. Streetman, Temperature, stress, and annealing effects on the luminescence from electron-irradiated silicon, *J. Appl. Phys.* **44**, 5402 (1973).
- [12] C. Chartrand, L. Bergeron, K. Morse, H. Riemann, N. Abrosimov, P. Becker, H.-J. Pohl, S. Simmons, and M. Thewalt, Highly enriched si 28 reveals remarkable optical linewidths and fine structure for well-known damage centers, *Phys. Rev. B* **98**, 195201 (2018).
- [13] L. Bergeron, C. Chartrand, A. Kurkjian, K. Morse, H. Riemann, N. Abrosimov, P. Becker, H.-J. Pohl, M. Thewalt, and S. Simmons, Silicon-integrated telecommunications photon-spin interface, *PRX Quantum* **1**, 020301 (2020).
- [14] D. B. Higginbottom, A. T. Kurkjian, C. Chartrand, M. Kazemi, N. A. Brunelle, E. R. MacQuarrie, J. R. Klein, N. R. Lee-Hone, J. Stacho, M. Ruether, *et al.*, Optical observation of single spins in silicon, *Nature* **607**, 266 (2022).
- [15] A. Johnston, U. Felix-Rendon, Y.-E. Wong, and S. Chen, Cavity-coupled telecom atomic source in silicon, *Nat. Commun.* **15**, 2350 (2024).
- [16] C.-M. Lee, F. Islam, S. Harper, M. A. Buyukkaya, D. Higginbottom, S. Simmons, and E. Waks, High-efficiency single photon emission from a silicon t-center in a nanobeam, *ACS Photon.* **10**, 3844 (2023).
- [17] F. Islam, C.-M. Lee, S. Harper, M. H. Rahaman, Y. Zhao, N. K. Vij, and E. Waks, Cavity-enhanced emission from a silicon t center, *Nano Lett.* **24**, 319 (2023).
- [18] L. Komza, X. Zhang, H. Song, Y.-L. Tang, X. Wei, and A. Sipahigil, Multiplexed color centers in a silicon photonic cavity array, arXiv preprint arXiv:2501.17339 (2025).
- [19] H. Song, X. Zhang, L. Komza, N. Fiaschi, Y. Xiong, Y. Zhi, S. Dhuey, A. Schwartzberg, T. Schenkel, G. Haupert, *et al.*, Long-lived entanglement of a spin-qubit register in silicon photonics, arXiv preprint arXiv:2504.15467 (2025).
- [20] A. N. Vamivakas, C.-Y. Lu, C. Matthiesen, Y. Zhao, S. Fält, A. Badolato, and M. Atatüre, Observation of spin-dependent quantum jumps via quantum dot resonance fluorescence, *Nature* **467**, 297 (2010).
- [21] A. Delteil, W.-b. Gao, P. Fallahi, J. Miguel-Sanchez, and A. Imamoğlu, Observation of quantum jumps of a single quantum dot spin using submicrosecond single-shot optical readout, *Phys. Rev. Lett.* **112**, 116802 (2014).
- [22] L. Robledo, L. Childress, H. Bernien, B. Hensen, P. F. Alkemade, and R. Hanson, High-fidelity projective readout of a solid-state spin quantum register, *Nature* **477**, 574 (2011).
- [23] D. D. Sukachev, A. Sipahigil, C. T. Nguyen, M. K. Bhaskar, R. E. Evans, F. Jelezko, and M. D. Lukin, Silicon-vacancy spin qubit in diamond: a quantum memory exceeding 10 ms with single-shot state readout, *Phys. Rev. Lett.* **119**, 223602 (2017).
- [24] M. Raha, S. Chen, C. M. Phenicie, S. Ourari, A. M. Dibos, and J. D. Thompson, Optical quantum nondemolition measurement of a single rare earth ion qubit, *Nat. Commun.* **11**, 1605 (2020).
- [25] J. M. Kindem, A. Ruskuc, J. G. Bartholomew, J. Rochman, Y. Q. Huan, and A. Faraon, Control and single-shot readout of an ion embedded in a nanophotonic cavity, *Nature* **580**, 201 (2020).
- [26] E. I. Rosenthal, S. Biswas, G. Scuri, H. Lee, A. J. Stein, H. C. Kleidermacher, J. Grzesik, A. E. Rugar, S. Aghaeimeibodi, D. Riedel, *et al.*, Single-shot readout and weak measurement of a tin-vacancy qubit in diamond, *Phys. Rev. X* **14**, 041008 (2024).
- [27] R. E. Evans, M. K. Bhaskar, D. D. Sukachev, C. T. Nguyen, A. Sipahigil, M. J. Burek, B. Machielse, G. H. Zhang, A. S. Zibrov, E. Bielejec, *et al.*, Photon-mediated interactions between quantum emitters in a diamond nanocavity, *Science* **362**, 662 (2018).
- [28] M. K. Bhaskar, R. Riedinger, B. Machielse, D. S. Levonian, C. T. Nguyen, E. N. Knall, H. Park, D. Englund, M. Lončar, D. D. Sukachev, *et al.*, Experimental demonstration of memory-enhanced quantum communication, *Nature* **580**, 60 (2020).
- [29] B. J. Shields, Q. P. Unterreithmeier, N. P. de Leon, H. Park, and M. D. Lukin, Efficient readout of a single spin state in diamond via spin-to-charge conversion, *Phys. Rev. Lett.* **114**, 136402 (2015).
- [30] C. P. Anderson, E. O. Glen, C. Zeledon, A. Bourassa, Y. Jin, Y. Zhu, C. Vorwerk, A. L. Crook, H. Abe, J. Ul-Hassan, *et al.*, Five-second coherence of a single spin with single-shot readout in silicon carbide, *Sci. Adv.* **8**, eabm5912 (2022).
- [31] P. Inc, F. Afzal, M. Akhlaghi, S. J. Beale, O. Bedroya, K. Bell, L. Bergeron, K. Bonsma-Fisher, P. Bychkova, Z. M. Chaisson, *et al.*, Distributed quantum computing in silicon, arXiv preprint arXiv:2406.01704 (2024).
- [32] J. R. Johansson, P. D. Nation, and F. Nori, Qutip: An open-source python framework for the dynamics of open quantum systems, *Comput. Phys. Commun.* **183**, 1760 (2012).
- [33] H. Goto, S. Mizukami, Y. Tokunaga, and T. Aoki, Figure of merit for single-photon generation based on cavity quantum electrodynamics, *Phys. Rev. A* **99**, 053843 (2019).
- [34] C. Bowness, S. A. Meynell, M. Dobinson, C. Clear, K. Jooya, N. Brunelle, M. Keshavarz, K. Boos, M. Gascoigne, S. Taherizadegan, *et al.*, Laser-induced spectral diffusion and excited-state mixing of silicon t centres, arXiv preprint arXiv:2504.09908 (2025).

- [35] X. Zhang, N. Fiaschi, L. Komza, H. Song, T. Schenkel, and A. Sipahigil, Laser-induced spectral diffusion of t centers in silicon nanophotonic devices, arXiv preprint arXiv:2504.08898 (2025).
- [36] C. W. Gardiner and M. J. Collett, Input and output in damped quantum systems: Quantum stochastic differential equations and the master equation, Phys. Rev. A **31**, 3761 (1985).
- [37] S. C. Endres, C. Sandrock, and W. W. Focke, A simplicial homology algorithm for lipschitz optimisation, J. Glob. Optim. **72**, 181 (2018).
- [38] E. Waks and J. Vuckovic, Dipole induced transparency in drop-filter cavity-waveguide systems, Phys. Rev. Lett. **96**, 153601 (2006).
- [39] C. P. Anderson, A. Bourassa, K. C. Miao, G. Wolfowicz, P. J. Mintun, A. L. Crook, H. Abe, J. Ul Hassan, N. T. Son, T. Ohshima, *et al.*, Electrical and optical control of single spins integrated in scalable semiconductor devices, Science **366**, 1225 (2019).
- [40] T. Schröder, M. E. Trusheim, M. Walsh, L. Li, J. Zheng, M. Schukraft, A. Sipahigil, R. E. Evans, D. D. Sukachev, C. T. Nguyen, *et al.*, Scalable focused ion beam creation of nearly lifetime-limited single quantum emitters in diamond nanostructures, Nat. Commun. **8**, 15376 (2017).
- [41] D. M. Toyli, C. D. Weis, G. D. Fuchs, T. Schenkel, and D. D. Awschalom, Chip-scale nanofabrication of single spins and spin arrays in diamond, Nano Lett. **10**, 3168 (2010).
- [42] A. Bourassa, C. P. Anderson, K. C. Miao, M. Onizhuk, H. Ma, A. L. Crook, H. Abe, J. Ul-Hassan, T. Ohshima, N. T. Son, *et al.*, Entanglement and control of single nuclear spins in isotopically engineered silicon carbide, Nat. Mater. **19**, 1319 (2020).
- [43] S. Ourari, L. Dusanowski, S. P. Horvath, M. T. Uysal, C. M. Phenicie, P. Stevenson, M. Raha, S. Chen, R. J. Cava, N. P. de Leon, *et al.*, Indistinguishable telecom band photons from a single er ion in the solid state, Nature **620**, 977 (2023).
- [44] S. Sun, J. L. Zhang, K. A. Fischer, M. J. Burek, C. Dory, K. G. Lagoudakis, Y.-K. Tzeng, M. Radulaski, Y. Keleita, A. Safavi-Naeini, *et al.*, Cavity-enhanced raman emission from a single color center in a solid, Phys. Rev. Lett. **121**, 083601 (2018).
- [45] P.-J. Stas, Y. Q. Huan, B. Machielse, E. N. Knall, A. Suleymanzade, B. Pingault, M. Sutula, S. W. Ding, C. M. Knaut, D. R. Assumpcao, *et al.*, Robust multi-qubit quantum network node with integrated error detection, Science **378**, 557 (2022).